American Journal of Physical Chemistry
2014; 3(6): 102-108
Published online December 18, 2014 (http://www.sciencepublishinggroup.com/j/ajpc)
doi: 10.11648/j.ajpc.20140306.13
ISSN: 2327-2430 (Print); ISSN: 2327-2449 (Online)

A novel visible– light driven photocatalyst: Ethylene glycol–citrate sol–gel synthesis, microwave–assisted calcination, and photocatalytic efficiency

Hakim Qaid Naji Museed Alarique[1, *], Elyas Sadeq Al-Aghbari[2], Niyazi Abdulmawla Sallam Al–Areqi[2, *], Ahlam Al–Alas[2], Khalid Ahmed Saeed Ghaleb[2]

[1]Department of Chemistry, Faculty of Education, Taiz University, Taiz, Yemen
[2]Department of Chemistry, Faculty of Applied Science, Taiz University, Taiz, Yemen

Email address:

hakim.alariqe@yahoo.com (H. Q. N. M. Alarique), niyazi.alareqi@gmail.com (N. A. S. Al–Areqi)

To cite this article:

Hakim Qaid Naji Museed Alarique, Elyas Sadeq Al-Aghbari, Niyazi Abdulmawla Sallam Al–Areqi, Ahlam Al–Alas, Khalid Ahmed Saeed Ghaleb. A Novel Visible– Light Driven Photocatalyst: Ethylene Glycol–Citrate Sol–Gel Synthesis, Microwave–Assisted Calcination, and Photocatalytic Efficiency. *American Journal of Physical Chemistry.* Vol. 3, No. 6, 2014, pp. 102-108. doi: 10.11648/j.ajpc.20140306.13

Abstract: A novel visible– light driven photocatalyst, BIMNVOX.*x* was synthesized by ethylene glycol–citrate sol–gel route and microwave- assisted calcination. The phocatalyst was characterized structurally by X–ray powder diffraction (XRPD) and simultaneous thermogravimetric–differential thermal analysis (TG–DTA). Its optical and surface properties were determined by means of UV–vis absorption spectrophotometry and BET– nitrogen adsorption isotherm measurements, respectively. The photocatalytic efficiency of BIMNVOX.x system was investigated by applying the pseudo first- order kinetic model to the photocatalytic degradation reaction of crystal violet, CV dye in aqueous solution under visible light irradiation. The β (orthorhombic) –BIMNVOX phase, space group Acam exhibited the highest photocatalytic degradability, indicating that the photocatalytic efficiency of BIMNVOX catalyst is essentially enhanced by the increased number of catalyst active sites, irrespective of the kind of phase stabilized and the increasing photoabsorption ability with Mn dopant content. Moreover, the possible photocatalytic degradation mechanism of aqueous CV dye solution under visible light irradiation was also proposed.

Keywords: Photocatalyst, BIMNVOX, Microwave- Assisted Calcination, Crystal Violet, Perovskites

1. Introduction

Dye pollutants released with industrial wastewater are an important source of environmental concern. Organic dyes are widely used in industrial processes and domestic activities, leading to esthetic pollution, eutrophication, and perturbations in aquatic life [1,2]. Crystal violet (CV) is a member the triphenylmethane family of dyes that has several industrial and biological applications. This large family is used extensively in a variety of industrial process, but many are also known to have carcinogenic and mutagenic properties[3,4]. Advanced oxidation processes (AOPs) have been proposed and widely investigated for the photodegradation of organic dyes in industrial wastewaters. Semiconductor mediated photocatalysis has been found to be potentially advantageous, as it costs less money and does not create secondary contamination [5]. Among known semiconductor photcatalysts, TiO_2 has been extensively studied for photocatalytic and photochemical applications because of its thermal stability, facile synthesis, low cost and the low toxicity (Zhang et al. 2006). However, because of its relatively high band–gap, TiO_2 (3.2 eV) is activated only by ultraviolet light with wavelengths shorter than 387 nm [6,7], which severely limits its commercial application for water and wastewater treatment. Hence, many researches have been devoted to find, design and optimize efficient semiconductor photocatalysts with maximum absorption thresholds (minimum band gaps) that effectively accelerate the photocataltyic degradation of organic dyes, when irradiated in the visible light region.

Very recently, a layered perovskite– type $Bi_4V_2O_{11}$ oxide and its metal– doped analogues, designated as BIMEVOX.*x* ($Bi_2Me_x^lV_{1-x}O_{5.5-(5-l)x/2}$; *l*=*Me* oxidation state) belonging to the Aurivillius family, have attracted considerable attention

due to their interesting propriety, such as in peculiar polymorphic structure and stability [8,9,10], very low electrical conductivity below 300 ^{o}C [11], reasonable scale–electronic and ferroelectric contribution at low dopant concentrations [12,13], and remarkably narrow band gap with a potential visible light photocatalytic efficiency [14,15]. BIMEVOX materials, such as BIALVOX, BIGAVOX [14] and BINIVOX [16] have shown enhanced photocatalytic degradation of some organic dyes in the visible spectral range as a consequence of band gap narrowing of the doped photocatalysts.

In the present paper, we report a novel visible– light driven photocatalyst, BIMNVOX.x $Bi_2Mn_x^{(IV)}V_{1-x}O_{5.5-(x/2)}$ for the photodegradation of organic dyes in industrial wastewaters. A series of BIMNVOX.x was synthesized by ethylene glycol–citrate sol–gel route and the resulting V and Mn containing xerogels were calcined by the microwave heating using a modified domestic microwave oven. The photocatalytic properties of the BIMNVOX.x catalyst were then investigated on the photodegradation of *CV* dye under visible light irradiation.

2. Experimental

2.1. Catalyst Preparation

Analytical grade $Bi(NO_3)_3.5H_2O$, NH_4VO_3 and $Mn(NO_3)_2.4\ H_2O$ were used as starting materials. Stock solutions of the starting materials (0.1 M) were prepared by dissolving an accurately weighed amount of corresponding material in deionized water. A 0.2 M citric acid solution used as chelating agent was prepared in deionized water– ethylene glycol mixture at a volumetric ratio of 3:1. A 0.5 M NH_3 solution was also used for adjusting pH.

The starting materials solutions were mixed at a volumetric ratio of 2: x: (1–x) = Bi: Mn: V with citric acid solution to form sol solutions. The ratio of citric solution to total metal ions was set at 1.5:1. The pH of resulting sol solutions were adjusted to ~7 by adding ammonia solution. The sol solutions were then heated at 80^{o}C under constant stirring for two hrs to form visible gel. Wet gels were further dehydrated in an oven at 90^{o}C for 12 hrs to remove excess water and obtain dried xerogels.

The xerogel was thoroughly mixed in an agate mortar for further homogenization and then divided into two equal portions. The first portion was thermally calcined in a muffle furnace at 550^{o}C for 6 hrs, while the second portion is subjected to a microwave–assisted calcination for 25 min in a modified microwave oven operated at a frequency of 2.45 GHz.

2.2. Structural Characterization of Photocatalyst

The stabilized phases and crystallite sizes for synthesized samples of photocatalyst were determined by the X–ray powder diffraction (XRPD) patterns obtained from a Rigaku/Max–B X–ray diffractometer using Ni–filtered CuK_α radiation. The diffraction beams were collected using a $\theta/2\theta$ geometry in the range of $15^{o} \leq 2\theta \leq 80^{o}$ with an increment of 0.05^{o} at scantime of 0.8 sec/increment. The unit cell parameters were refined using an *X'Pert Plus* software program. The average crystallite size was calculated from the diffraction line broadening via the Scherrer equation:

$$D = \frac{0.89\lambda}{B\cos\theta} \quad (1)$$

where D is the crystal size in nm, λ is the CuK_α radiation wavelength (λ=1.54060Å), B is the half–width of the peak in radians and θ is the corresponding diffraction angle.

The thermal decomposition of xerogel and the polymorphic structure were investigated by thermogravimetric – differential thermal analysis (TG–DTA) using a Perkin Elmer thermal analyzer at a heating rate of 10 ^{o}C min^{-1}, running up to 1000^{o}C with an air flow rate of 30 ml min^{-1}. α–alumina was used as a reference material. The microwave- assisted decomposition of xerogel as a function of calcination time was also followed by the X–ray powder diffraction.

2.3. Optical and Surface Properties of Photocatalyst

The optical band– gap energies (E_g) for the photocatalyst series were estimated from UV–vis absorption spectra, collected on a Shimadzu Scan UV–vis spectrophotometer (UV–1240) at room temperature in the wavelength range 200–750 nm. The direct band– gap energy was calculated from the wavelength corresponding to the band–gap edge absorption ($\lambda_{ab(g)}$) using equation (2) [17]:

$$E_g(eV) = \frac{1240}{\lambda_{ab(g)}(nm)} \quad (2)$$

Surface area measurements were performed by nitrogen adsorption– desorption isotherm at 77 K on an Autosorb–1(Quantachrome) adsorption apparatus. The adsorption data were collected in the nitrogen partial pressure (P/P_o) range of 0.01–0.99. The specific surface areas (S_{BET}) expressed in m^2/g, were calculated by Brunauer–Emmett–Teller (BET) method.

2.4. Photocatalytic Activity Measurements

A 250–ml aqueous solution of CV dye (5×10^{-4} M) at pH ~10.0 (adjusted with diluted aqueous solution of NH_3 and H_2SO_4) was placed in a 450 ml – photoreactor equipped with a magnetic stirrer. Before photocatalytic reaction, 200–mg powdered sample of the photocatayst was dispersed in the dye aqueous solution. The resulting suspension was then magnetically stirred in the dark for 25 min to reach the adsorption–desorption equilibrium. The visible light with wavelengths greater than 400 nm using a 300–W Xe lamp was irradiated perpendicularly to the surface of solution at affixed distance between the visible source and the surface of dye solution (25 cm). At specific time intervals (10 min) about 5 ml– aliquot of the reaction mixture was withdrawn from the photoreactor and then filtered to separate the catalyst residues. The concentrations of dye versus irradiation time were

determined by measuring the maximum absorbance (λ_{max}=590 nm) using a Shimadzu UV–vis spectrophotometer (UV–1240). The photocatalytic activity of the BIMNVOX.*x* catalyst as a function of composition for the dye photodegradation was investigated using a pseudo first– order kinetic model.

$$ln(C_t / C_o) = -k_{app}\ t \qquad (3)$$

where C_o and C_t are the initial concentration and concentration at time, *t* of CV dye solution, respectively and k_{app} denotes the apparent first– order rate constant.

3. Results and Discussion

3.1. Structural and Polymorphic Properties of Photocatalyst

Figure 1 presents TG–DTA thermogram of BMNVOX.13 xerogel, which clearly shows a two–step thermal degradation, starting from 77 °C and extending upto 449 °C. Two thermal events are accompanied with the overall decomposition; a small endothermic and sharper exothermic peak which are observed at 192 °C and 449 °C, respectively. However, the first weight loss of the thermal degradation (~5.4 %), corresponding to the endothermic peak is attributed to elimination of physically adsorbed ammonia and water from the xerogel. It is also possible that free ammonium citrate and ethylene glycol are partially decomposed in this step. The second weight loss (~ 41.3 %), corresponding to the exothermic peak is associated with a fast decomposition and decarbonization of chelating citrate and ethylene glycol [13,18].

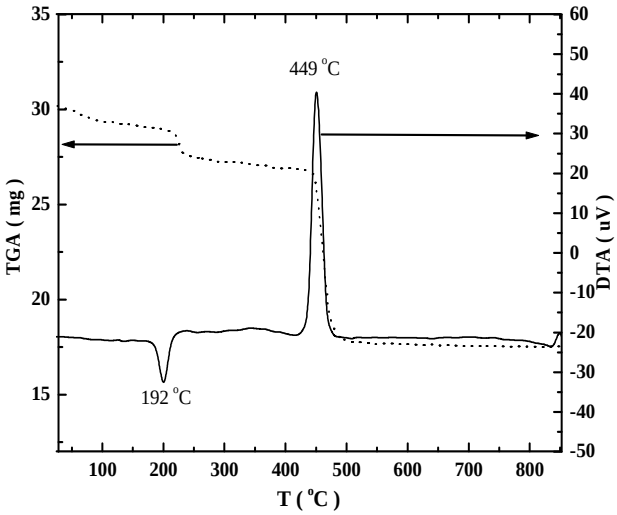

Figure 1. *TG–DTA thermogram of as–prepared BIMNVOX.13 xerogel.*

The variation of XRPD patterns of the BIMNVOX.13 xerogel with time of microwave–assisted calcination at 2.45 GHz are presented in Figure 2. It can be observed that the xerogel is calcined and well- crystallized under microwave heating for 25 min as clearly evidenced by the existence of a characteristic singlet diffraction peak 110 around 2θ ~ 32.5°.

Figure 3 present the XRPD patterns of as– synthesized BIMNVOX.*x* photocatalyst doped with varying Mn concentration. It can be noted that no significant polymorphism occurs in the substituted system with increasing Mn content upto $x < 0.10$. For compositions with $x = 0.10$, the singlet indexed 220, shows the existence of orthorhombic β–BIMNVOX phase of higher symmetry having space group *Acam* [19]. However for $x \geq 0.13$, the tetragonal γ′–BIMNVOX.13 phase, space group, *I4/mmm* is stabilized as clearly evidenced by the convergence of the sub–lattice doublet ca. $2\theta \sim 32.5^o$ into a singlet indexed in tetragonal cell as (110) at $2\theta \sim 32^o$ [20]. It is worthwhile to appoint that our structural characterization is found to be in a perfect agreement with what have been reported earlier for the BIMNVOX system [21].

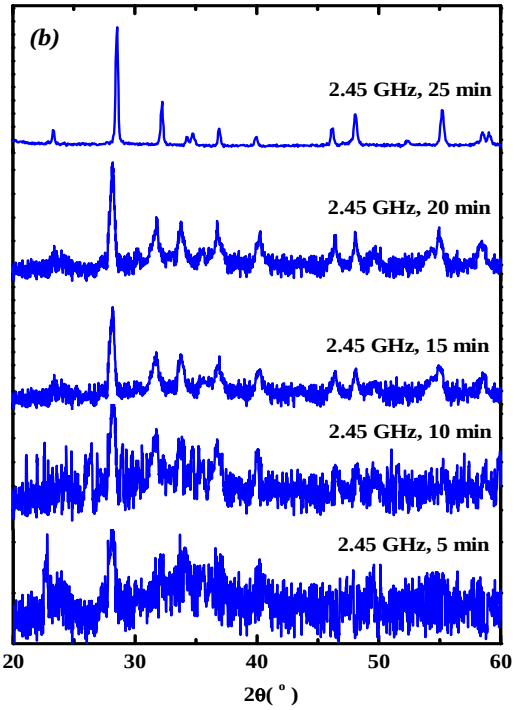

Figure 2. *XRPD patterns of the BIMNVOX.13 xerogel calcined by microwave –assisted route at 2.45 GHz as a function of time.*

Values of unit cell refinement, average crystallite size and crystallographic density obtained from fitting diffraction patterns are listed in Table 1. It is clear that the substitution of Mn into the $Bi_4V_2O_{11}$ compound causes a dramatic increase in the unit cell dimensions, accompanied by the same trend in the overall cell volume. The density and particle size both are found to increase slightly with the increase of Mn dopant content. This trend is in a good agreement with the variation of unit cell parameters, and reflecting the positive contribution of Mn substitution to the overall lattice expansion as a result of the incorporation of Mn (IV) dopant ions of larger ionic radius (0.72 Å) into the perovskite vanadate layers in the place of pentavalent vanadium sites (0.54 Å) as revealed earlier [22].

DTA thermograms depicts thermal stability of the BIMNVOX.*x* system and onset temperature of phase transitions (Figure 4). The two characteristic endothermic peaks clearly seen for the parent compound, $Bi_4V_2O_{11}$ (*x*=0) as

well as the substituted photocatalyst with composition, x=0.05 are attributed to the consequent α→β and and β→γ transitions [23-25]. In addition, the heat flow per unit mass of the α→β

Table 1. *Refined unit cell parameters, crystallographic densities, average crystallite sizes and specific surface areas of as–prepared BIMNVOX.x photocatalyst series.*

x	Unit cell parameters				d_{XRPD} (g cm^{-3})	Average crystallite size (μm)	BET surface area (m^2/g)
	a(Å)	b(Å)	c (Å)	V(Å^3)			
0.00	5.521	5.627	15.293	475.10	6.78	4.12	0.21
0.05	5.611	5.623	15.387	485.47	6.83	4.24	0.19
0.10	5.624	5.633	15.453	489.55	6.97	4.37	0.24
0.13	5.631	–	15.508	491.73	7.12	4.56	0.23

transition is found to be nearly three orders of magnitude higher than that of the β→γ transition. However, the β–BIMNVOX.10 photocatalyst shows a single endothermic peak 469 °C, assigned to the β→γ transition, while the occurrence of order → disorder, γ'→γ transition is observed for the γ'–BIMNVOX.13 phase [25, 26].

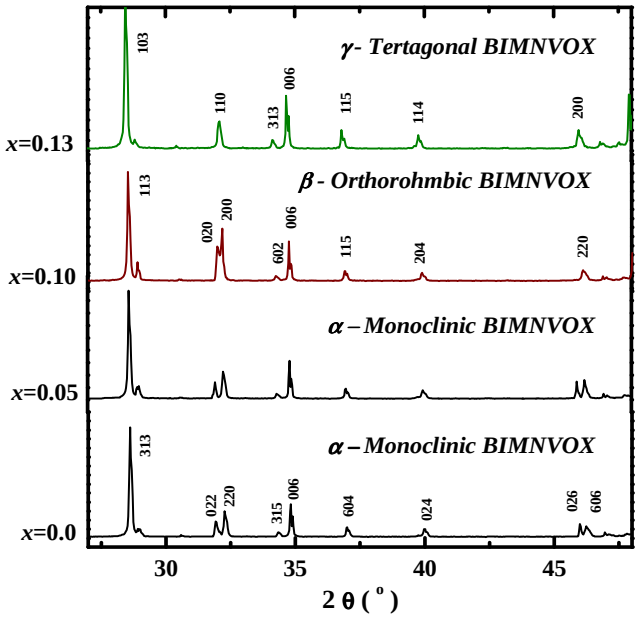

Figure 3. *XRPD patterns of as–synthesized BIMNVOX.x photocatalyst series.*

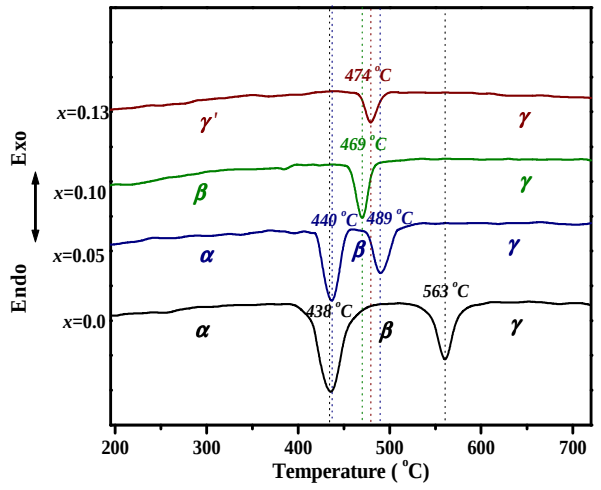

Figure 4. *DTA thermograms of as– synthesized BIMNVOX.x photocatalyst series.*

3.2. Optical and Surface Properties of Photocatalyst

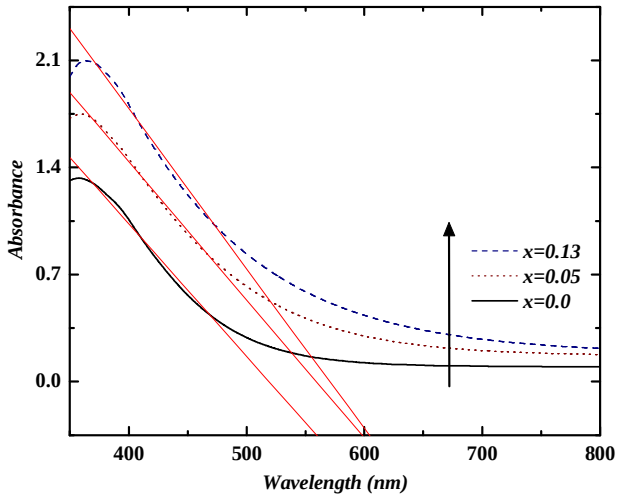

Figure 5. *UV–vis spectra of the BIMNVOX.x photocatalyst.*

UV–vis absorption spectra of BIMNVOX.x photocatalyst for various compositions are presented in Figure 5. The intrinsic band– gap absorption of $Bi_4V_2O_{11}$ is clearly seen at ~ 559 nm, resulting from the electronic transitions from *Bi6s/O2p* orbitals of the bismuthate $(Bi_2O_2)^{2+}$ layers (valence band) to *V3d* orbitals of the $(VO_{3.5}\square_{0.5})^{2-}$ perovskite– like slabs (conduction band) [14, 15], where $\square$ represents an oxygen vacancy in vanadate polyhydra. The absorption edges of the BIMNVOX.x photocatalysts are found to shift toward longer wavelengths as the concentration of Mn dopant increases. This is without a doubt attributed to the additional contribution of *Mn3d* orbitals to the conduction band [16] and increasing oxygen vacancy concentration [24, 27] in the perovskite vanadate layers. The variation of the optical band–gap energy of the BIMNVOX.x catalyst with Mn dopant concentration is illustrated in Table 2. It can be noted that the absorption edge of the BIMNVOX system is shifted towards the visible light region with the increasing Mn content compared to the pure $Bi_4V_2O_{11}$. However this narrowing of band– gap energies is also accompanied by an increase in the specific surface areas (S_{BET}), suggesting that the Mn– doping strategy might play a positive contribution to the photoabsorption and photocatalytic activities of doped photocatalyst. This behaviour may be explained by the fact that the increasing Mn substitution leads to creation of oxygen vacancies at the equatorial planes of perovskite vanadate layers [13, 28]. Such oxygen vacancies not only extend the

optical absorption edge into the visible light region, but also serve as active sites available for the dye molecules to adsorb on the surface of photocatalysts and due to which their photocatalytic degradation becomes effectively enhanced [29].

Table 2. *Values of band– gap energy for the BIMNVOX.x photocatalyst*

x	$\lambda_{ab(nm)}$	E_g (eV)	SD	R^2
0.00	559.08	2.22	0.03544	0.9925
0.05	597.91	2.07	0.02446	0.9967
0.13	604.58	2.05	0.04114	0.99457

3.3. Photocatalytic Efficiency and Proposed Mechanism

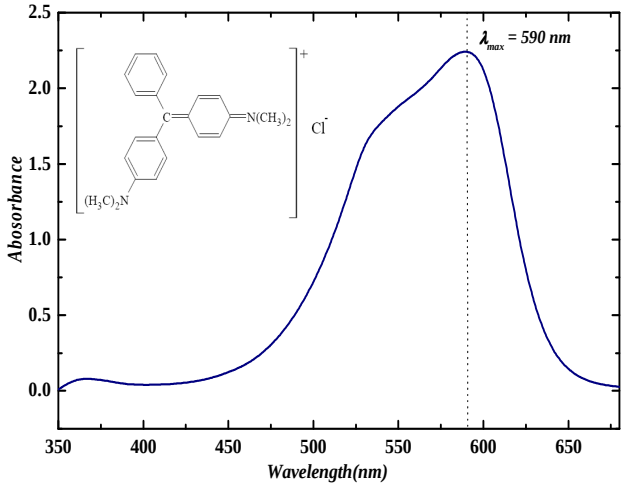

Figure 6. *UV–vis spectrum of CV dye.*

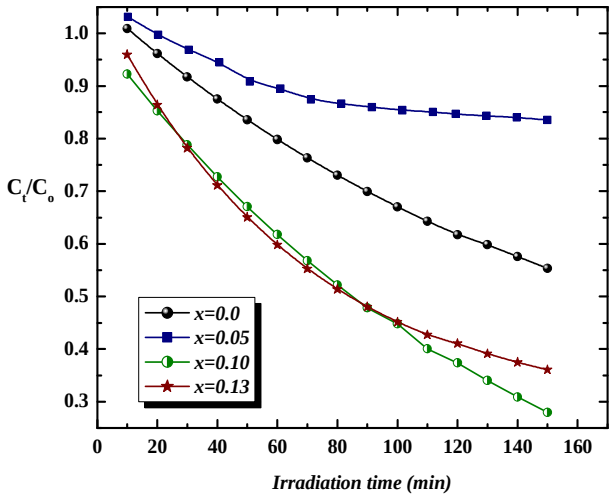

Figure 7. *Photocatalytic activities of the BIMNVOX.x catalyst series for the degradation of CV dye solution under visible light irradiation.*

The UV–vis spectrum of *CV* dye solution before photolysis and photocatalytic degradation, shows a main absorbance in visible light region at 590 nm (Figure 6). Thus, the values of C_o and C_t were obtained from the corresponding absorbance, measured at this wavelength. The variation in the photocatalytic degradation efficiency of *CV* dye with pure $Bi_4V_2O_{11}$ and doped BIMNVOX.*x* samples at varying Mn concentration is presented in Figure 7. It can be observed that the photodegradation of *CV* dye proceeds more rapidly when catalyzed by the BIMNVOX.*x* system, whose Mn content lies in the compositional range of the β– phase stabilization. It is worthwhile to appoint that this result is contrary to what have been reported very earlier for the BINIVOX.*x* photocatalyst [16], where compositions with stabilized γ– phase have shown a maximal photocatalytic efficiency.

The values of k_{app} (min^{-1}) were calculated from the slope using the line–regression fitting to the first– order kinetic model as shown in Figure 8. Table 3 illustrates the variation of k_{app} with Mn dopant level incorporated in the photocatalyst along with the regression determination coefficients (R^2). The highest photocatalytic degradability exhibited by the BIMNVOX catalyst with stabilized β− phase (k_{app} = 8.45×10^{-3} min^{-1} for x=0.10) indicates that the photocatalytic efficiency of BIMNVOX catalyst is essentially enhanced by the increased number of catalyst active sites, irrespective of the kind of phase stabilized and the increasing photoabsorption ability with Mn dopant content. The important point to be emphasized here is that the number of photocatalyst active sites reaches its maximum at x=0.10, which is in a good agreement with the expected optimal concentration of oxygen vacancies created at the equatorial planes the perovskite vanadate layers. This can also be evidenced by the lowering in the photocatalytic activity beyond this value of Mn content (k_{app} = 6.96×10^{-3} min^{-1} for x=0.13).

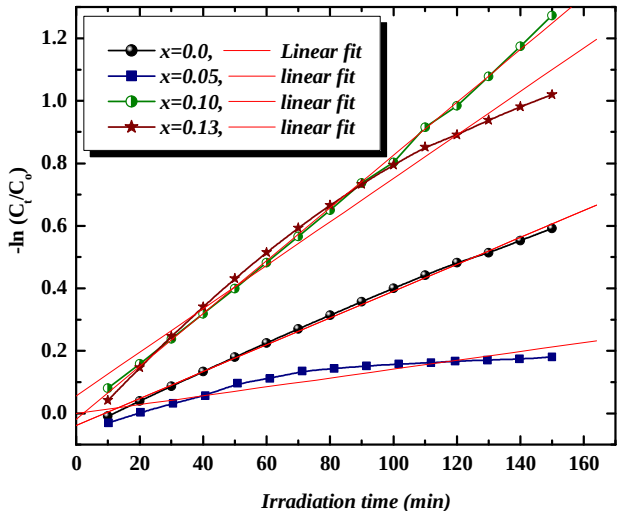

Figure 8. *Linear least– squares fitted plots of ln (C/C_o) versus irradiation time of the pseudo first–order kinetics for the visible– light photodegradation of CV dye catalyzed by various compositions of the BIMNVOX.x system.*

However, the decreased photocatalytic efficiency of γ −BIMNVOX.*x* catalyst for x=0.13, despite its highest ability to absorb visible light(E_g=2.05 *eV*), may be attributed to the creation of oxygen vacancies at apical positions of the perovskite vanadate layers [16,17]. These apical vacancies are not only considered as inactive sites on the photocatalyst surface, they may also play a role in the fast recombination of the electron–hole pairs, and thereby slowing down the photocatalytic degradation.

Table 3. *Variation in the rate constant of photocatalytic degradation of CV dye as a function of Mn substitution in BIMNVOX.x catalyst.*

x	k_{app} (min^{-1}) × 10^{-3}	SD	R^2
0.00	4.30	0.0091	0.99896
0.05	1.42	0.02543	0.9324
0.10	8.45	0.01201	0.99953
0.13	6.96	0.04992	0.98826

The photocatalytic mechanism of *CV* dye degradation using the BIMNVOX.*x* catalyst under visible light irradiation can be explained by the fact that the Mn doping initially narrows the band gap of the photocatalysts to enhance visible light absorption [17]. The *CV* dye molecules are then adsorbed onto the perovskite vanadate layers as a result of a coulombic interaction between negatively charged oxygen atoms of the vanadate layers and the dye molecules with positively conjugated chromophore. Under irradiated visible light energy, the mechanism suggests that excitation of the adsorbed *CV* dye takes place by visible light absorption to the appropriate singlet or triplet states, subsequently followed by electron ejection from the excited dye molecule onto the conduction band, while the dye is converted into a cationic dye radical ($CV^{\bullet+}$) that undergoes degradation to yield mineralization products. The dye photocatalytic degradation reactions can be schematically summarized in Figure 9 [16, 29- 31]. The resulting radical ($OH^{\cdot}$), being a very strong oxidizing agent (standard redox potential +2.8 V) can oxidize most dyes to the mineral end products.

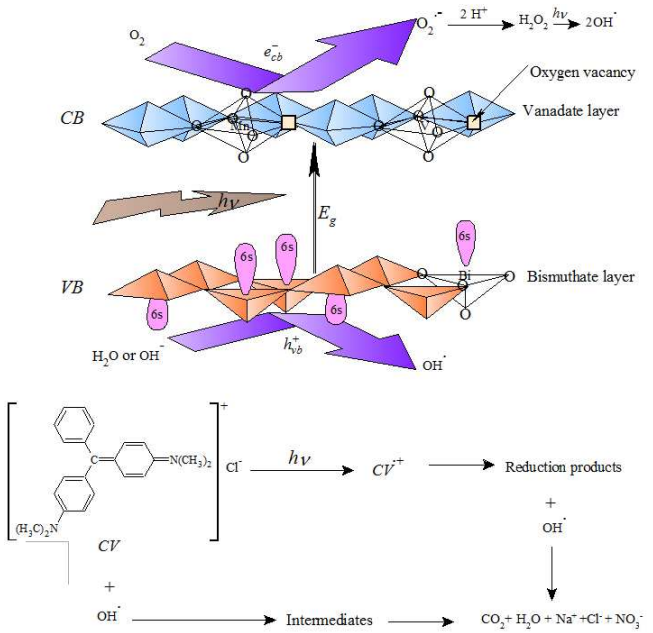

Figure 9. *Proposed mechanism of CV dye degradation by BINIVOX.x photocatalyst under visible light irradiation.*

4. Conclusions

A novel Aurivillius– type BIMNVOX.*x* photocatalyst was successfully synthesized by ethylene glycol–citrate sol–gel route and microwave- assisted calcination. It has been found that the increase of Mn (VI) dopant content (*x*) in the BIMNVOX.*x* photocatalyst result in narrowing of band– gap energies, accompanied by the increase in the specific surface areas (S_{BET}), and thereby enhancing the photoabsorption and photocatalytic activities of doped photocatalyst. It is interesting to note that the highest photocatalytic degradability, exhibited by the β− stabilized BIMNVOX.*x* phase for *x*=0.10, indicates that the enhancement of photocatalytic efficiency of BIMNVOX catalyst is attributed to the optimal concentration of oxygen vacancies (catalyst active sites) created at the equatorial planes of the perovskite vanadate layers, irrespective of the kind of phase stabilized and the increasing photoabsorption ability with Mn dopant content.

Acknowledgements

The authors are pleased to acknowledge Prof. Saba Beg, Department of Chemistry, Aligarh Muslim University (AMU), Aligarh (U.P.) – India for providing research facilities.

References

[1] Mckay, G.; Porter, J.F.; Prasad, G.R. 1998. The removal of dye colors from aqueous solutions by adsorption on low cost materials. Water Air Soil Pollut. 114, 423–438.

[2] Chen, C.C.; Chaudhary, A.J. & Grimes, S.M. 2005. Photodegradation of acid blue –29 and ethyl violet in the presence of NaOH and aluminum ions. J. Hazard. Mater. 117, 171–178.

[3] Littlefield, N.A.; Blackwell, B.N.; Hewitt, C.C. and Gaylor, D.W. 1985. Chronic toxicity and carcinogenicity studies of gentian violet in mice. Fundam. Appl. Toxicol. 5, 902–912.

[4] Chen, C–.Y. ; Kuo, J–.T.; Yang, H–.A. & Chung, Y–.C. 2013. A coupled biological and photocatalysis pretreatment system for the removal of crystal violet from wastewater. Chemosphere 92, 695–701.

[5] Mahmoodi, N. M.; Arami, M.; Limaee, N.Y. 2006. Photocatalytic degradation of triazinic ring–containing azo dye (Reactive Red 198) by using immobilized TiO_2 photoreactor: Bench scale study. J. Hazard. Mater. B133, 113–118.

[6] Legrini, O.; Oliveros, E. and Braun, A.M. 1993. Photochemical processes for water treatment. Chem. Rev. 93, 671–698.

[7] Konstantinou, I.K. & Albanis, T.A. 2004. TiO_2–assisted photocatalytic degradation of azo dyes in aqueous solution: kinetic and mechanistic investigations: A review. Appl. Catal. B: Environ. 49, 1–14.

[8] Abraham, F.; Debreuille– Gresse, M.F.; Mairesse, G. & Nowogrocki, G. 1988. Phase transition and ionic conductivity in $Bi_4V_2O_{11}$ An oxide with a layered structure. Solid State Ionics 28–30, 529–538.

[9] Boivin, J.C. & Mairesse, G. 1998. Recent developments in fast oxide ion conductors. Chem. Mater. 10, 2870–2888.

[10] Malys, M. ; Abrahams, I.; Krok, F.; Wrobel, W. & Dygas, J.R. 2008. The appearance of an orthorhombic BIMEVOX phase in the system $Bi_2Mg_xV_{1-x}O_{5.5-3x/2-\delta}$ at high values of *x*. Solid State Ionics 179, 82–87.

[11] Beg, S. & Al–Areqi, N.A.S. 2009. Structural and electrical study of Ce^{IV}–substituted bismuth vanadate. J. Phys. Chem. Solids 70, 1000–1007.

[12] Beg, S.; Al–Areqi, N.A.S. & Al–Alas, A. 2009. Composition dependance of phase transition and ionic conductivity in BIHFVOX system. J. Alloys Compds 479, 107–112.

[13] Beg, S.; Al–Alas, A. & Al–Areqi, N.A.S. 2010. Layered Aurivillius compound: Synthesis, characterization and electrical properties. J. Alloys and Compds 504, 413–419.

[14] Thakral, V. & Uma, S. 2010. Investigation of visible light photocatalytic behavior of $Bi_4V_2O_{11-\delta}$ and BIMEVOX (ME = Al, Ga) oxides. Mater. Res. Bull. 45, 1250–1254.

[15] Al–Areqi, N.A.S.; Al–Kamali, A.S.N.; Ghaleb, Kh.A.S.; Al–Alas A. & Al–Mureish, Kh. 2014. Influence of phase stabilization and perovskite vanadate oxygen vacancies of the BINIVOX catalyst on photocatalytic degradation of azo dye under visible light irradiation. Rad. Eff. Def. Solids 169, 117–128.

[16] Al–Areqi, N.A.S.; Al–Alas, A.; Al–Kamali, A.S.N.; Ghaleba, Kh.A.S. & Al–Mureish, Kh. 2014. Photodegradation of 4–SPPN dye catalyzed by Ni(II)–substituted $Bi_2VO_{5.5}$ system under visible light irradiation: Influence of phase stability and perovskite vanadate–oxygen vacancies of photocatalyst. J. Mol. Cata. A: Chem. 381, 1– 8.

[17] Zheng, Y.; Duan, F.; Chen, M.Q. & Xie, Y. 2010. Synthetic $Bi_2O_2CO_3$ nanostructures: novel photocatalyst with controlled special surface exposed. J. Mol. Catal. A: Chem. 317, 34–40.

[18] Hervoches, C.H. ; Steil, M.C.& Muccillo, R. 2004. Synthesis by the polymeric precursor technique of $Bi_2Co_{0.1}V_{0.9}O_{5.35}$ and electrical properties dependence on the crystallite size. Solid State Sci 6 (2004) 173–177.

[19] Li, E.J.; Xia, K.; Yin, S.F.; Dai, W. L.; Luo, S. L. & Au, C.T. 2010. Preparation, characterization and photocatalytic activity of Bi_2O_3–MgO composites. Mater. Chem. Phys. 125, 236–241.

[20] Krok, F.; Abrahams, I.; Zadrozna, A.; Małys, M.; Bogusz, W.; Nelstrop, J.A.G. & Bush, A.J. 1999. Electrical conductivity and structure correlation in BIMNVOX. Solid State Ionics 119, 139–144.

[21] Beg, S.; Hafiz, S. & Al–Areqi, N.A.S. 2011. Structural and electrical changes in BIMNVOX oxide– ion conductor. Def. Diff. Forum 316–317, 7–22.

[22] Al–Areqi, N.A.S. & Beg, S. 2009. Phase transition changes in $Bi_4Ce_xV_{2-x}O_{11-(x/2)-\delta}$ system. Mater. Chem. Phys. 115, 5–8.

[23] Shannon, R.D. & Prewitt, C.T. 1969. Effective ionic radii in oxides and fluorides. Acta Crystallogr. B 25, 925–946.

[24] Pernot, E.; Anne, M.; Bacmann, M.; Strobe1, P.; Fouletier, J.; Vannier, R.N.; Mairesse, G.; Abraham, F. & Nowogrocki, G. 1994. Structure and conductivity of Cu and Ni–substituted $Bi_2V_2O_{1\,1}$ compounds. Solid State Ionics 70–71, 259–263.

[25] Alga, M.; Ammar, A.; Essalim, R.; Tanouti, B.; Outzourhit, A.; Mauvy, F.& Decourt, R. 2005. Study on structural, thermal, sintering and conductivity of Cu–Co doubly substituted $Bi_4V_2O_{11}$. Ionics 11, 81–86.

[26] Watanabe, A. & Das, K. 2002. Time–dependent degradation due to the gradual phase change in BICUVOX and BICOVOX oxide–ion conductors at temperatures below about 500°C. J. Solid State Chem. 163, 224–230.

[27] Wrobel, W.; Abrahams, I.; Krok, F.; Kozanecka, A.; Malys, M.; Bogusz, W. & Dygas, J.R. 2004. Phase stabilization and electrical characterisation in the pseudo–binary system Bi_2ZrO_5–$Bi_2VO_{5.5-\delta}$. Solid State Ionics 175, 425–429.

[28] Abrahams, I. & Krok, F. 2002. Defect chemistry in the BIMEVOXes. J. Mater. Chem.12, 3351–3362.

[29] Yang, X.; Ma, F. Li, K.; Guo, Y.; Hu, J. Li, W.; Huo, M. & Guo, Y. 2010. Mixed phase titania nanocomposite codoped with metallic silver and vanadium oxide: New efficient photocatalyst for dye degradation. J. Hazard. Mater. 175, 429–438

[30] Im, J. S.; Bai, B. C.; In, S. J. & Lee, Y. S. 2010. Improved photodegradation properties and kinetic models of a solar–light–responsive photocatalyst when incorporated into electrospun hydrogel fibers. J. Colloid Interface Sci. 346, 216–221.

[31] Pouretedal, H. R. & Keshavarz, M. H. 2010. Synthesis and characterization of $Zn_{1-x}Cu_xS$ and $Zn_{1-x}Ni_xS$ nanoparticles and their applications as photocatalyst in Congo red degradation. J. Alloys Compds 501, 130–135.